Hindawi
Adsorption Science & Technology
Volume 2023, Article ID 6695350, 19 pages
https://doi.org/10.1155/2023/6695350

Research Article

Enhanced Adsorption of Rose Bengal Dye from Aqueous Solution Using NaOH Activated Hydrochar Derived from Corncob Waste

R. Sivaranjanee[1] **and P. Senthil Kumar**[2]

[1]*Department of Chemical Engineering, Sri Sivasubramaniya Nadar College of Engineering, Kalavakkam 603110, Tamil Nadu, India*
[2]*Centre for Pollution Control and Environmental Engineering, School of Engineering and Technology, Pondicherry University, Kalapet, Puducherry 605014, India*

Correspondence should be addressed to P. Senthil Kumar; senthilkumarp@pondiuni.ac.in

Received 25 July 2023; Revised 7 September 2023; Accepted 10 October 2023; Published 8 November 2023

Academic Editor: Muhammad Iqhrammullah

A potential approach to the preparation of affordable activated hydrochar is the hydrothermal carbonization of biomass wastes. In this study, hydrochar was made by hydrothermally carbonizing corncob wastes and then activating them with sodium hydroxide (NaOH). According to the findings, the adsorption capabilities of hydrochar generated at prolonged retention durations, lesser liquid-to-solid ratios, and elevated temperatures were considerably greater. The hydrochars were then analyzed utilizing a variety of characterization methods, and batch tests involving the sorption of rose bengal dye were carried out under a variety of conditions. According to the findings, activated hydrochar has a specific surface area of 12.794 m^2/g. In order to better understand and characterize the process of rose bengal dye adsorption, sorption kinetics, and sorption equilibrium onto the produced hydrochars, sorption kinetics and isotherms were further examined through experimental data fitting. The NaOH-activated hydrochar's adsorption capacity was 799.9 mg/g, respectively. The objective of this research was to assess the viability of using NaOH-activated hydrochar derived from corncobs as an economical and efficient sorbent for eliminating anionic dyes like rose bengal from aqueous solutions. Additionally, the study sought to investigate how various factors influence its sorption capabilities and to provide insights into the adsorption process through kinetic and isotherm analyses.

1. Introduction

This generation faces a serious problem with harmful substances like dyes, metal ions, and water pollution. More than 100 million people throughout the world do not have a source of safe drinking water, and it is predicted that this figure will increase by half in the coming years [1]. Water quality has been significantly impacted by industrial development, climate change, and rapid growth in population giving rise to an expanding freshwater crisis across the globe. Because of this, numerous freshwater polluters and consumers greatly impart to the exhaustion of freshwater [2]. Owing to the surplus utilization of water by households and other sectors, such origins turned into a regular location for getting rid of any product that affects the biota and ecosystem quality [3].

The most popular form of dye is xanthene dyes, which are distinguished by having an aromatic group as the chromophore in the xanthene's nucleus. The photochemical and textile industries frequently use the popular xanthene dye, rose bengal. The corneal epithelium in particular is seriously harmed by it. This dye may be exceedingly toxic and can cause blistering, reddening, inflammation, and itching once it is brought into interaction with the skin. It also affects the eyes, creating a variety of symptoms such as itching, redness, irritation, and more [4].

The processing of wastewater produced by the dyeing industries is also severely hampered by the fact that practically all dyes are either resistant to environmental factors or poorly recyclable [5]. At present, a variety of techniques are employed for treating the water that has been polluted. With the help of these methods, contaminants can be completely removed or have their concentrations reduced to within acceptable ranges. The price is still rather expensive, though. Thus, figuring out affordable techniques and

resources for the treatment of wastewater continues to remain a goal for industrials [6]. Traditional biological treatment methods cannot entirely eliminate dyes [5]. Adsorption is said to be the most efficient approach towards purifying water because of its practicality, simplicity of operation, and efficacy. In order to eliminate dye from water, a variety of substances have been utilized as adsorbents [7]. Hydrochar (HC) appears to be one of the adsorbents that are particularly effective in removing pollutants. Waste biomass, which mostly contains functional groups such as phenol, ether, carboxylic, ketones, aldehydes, and alcohol, has been employed as an adsorbent most frequently. These functional groups are essential for attaching the contaminant to the adsorbent's surface.

The adsorbents produced by the hydrothermal carbonization (HTC) of carbon-based precursors, such as lignocellulosic biomasses, are commonly referred to as "hydrochar." There are oxygenated functional groups like lactonic, carboxylic, and phenolic groups on the surface of HC made from raw materials comprising lignin, hemicellulose, and cellulose [8].

The quantity of residual biomass has been increasing quickly in recent times, yet it has been difficult to properly process or use it. Because this method is straightforward, inexpensive, and sustainable, it helps achieve the dual benefits of restoration of the habitat and waste treatment. Waste biomass is converted into hydrochar by HTC at a fairly low temperature [9].

HTC is a wet thermochemical technique that keeps water in liquid form for a short while to many hours with little to no oxygen exposure. It occurs at elevated pressures exceeding saturation pressures and temperatures between 180°C and 300°C [10]. Although the usage of subcritical water, whether it contains or lacks oxidants, is a well-known method of wastewater treatment, it has recently gained interest as a technique for converting biomass into HC [11]. This method is preferable to pyrolysis when using biomass with high moisture content [12]. By immersing the material being used in water and regulating the subcritical pressure and temperature, HTC may use substrates with an excessive or inadequate moisture content. The HTC technique is better suited because it is viable because the liquid fraction can be recirculated or reused into the process, minimizes the production of air pollutants, does not require predrying of the raw material, uses less energy because it runs at considerably lower temperatures between 150 and 375°C, and makes use of cheap and widely accessible materials that are renewable [13]. As the enhanced ionization constant facilitates processes that are typically catalyzed by bases and acids, under these circumstances, the dielectric constant of water is greatly lowered, providing characteristics equivalent to organic solvents at ambient temperature [14].

The two fundamental procedures for making activated carbon are activation and carbonization. Along with the kind of regeneration process, activation agent, and raw material, these stages mostly impact their cost and performance. In the course of the HTC process, the feedstock passes through a number of significant reactions [15]. Starting with hydrolysis, feedstock degradation is then dominated by reaction processes like recondensation, aromatization, decarboxylation, and dehydration [16].

The scientific community has taken notice of HC because of its excellent capabilities as a practical and environmentally friendly sorbent for expelling harmful substances from the aqueous phase [17]. Due to its strong capacity to eliminate pollutants from wastewater, HC had a better ability than biochar in eliminating both polar and nonpolar organic compounds [18]. The next-generation sustainable carbonaceous sorbent, known as HC, may be procured by HTC using any kind of raw material in place of previously employed traditional activated carbon. The raw material, retention time, and temperature of HTC have a significant impact on the structure and sorption capability of HC [19].

HTC hydrochar is created with limited aromatization, little ash, and a high carbon content, which results in a high oxygen functional group (OFG) level. On the other hand, as a result of porosity clogs primarily brought on by the process of hydrocarbon condensation on the HC's surface, the HTC approach produced HC with a relatively small pore size and a surface area that was smaller. This drawback requires that HC be modified or activated [20]. It was discovered that HC modification was the most efficient method for improving surface properties for effective pollutant elimination [12]. The selection of temperature and modifying chemicals used also influence how functional groups are modified and how porosity develops on char.

The typical low pore volume and surface area of HC would prevent it from being used as an adsorbent. Therefore, modification is required to enhance the sorption capacity of HC. The shape and structure of chars can be drastically altered by conventional char modification techniques including salts, bases, acids, steam, and CO_2 which may further impact their sorption effectiveness. The adsorptive characteristics of HC are expected to be enhanced by using each of these modification techniques [21].

Activation substantially enhances the sorption characteristics of hydrochar by augmenting its surface area, altering pore configurations, and increasing surface chemistry, resulting in elevated sorption capacities and rates. The selection of the activation technique and parameters can be customized according to the specific application and the pollutants in focus, thereby achieving the most effective outcomes.

Two methods of activation are available: Chemical activation involves modifying the HC sample using chemical activators to enhance its porous nature and specific surface area, which enhances its ability to adsorb contaminants [22]. Chemical activation using NaOH, $ZnCl_2$, H_3PO_4, and KOH commonly occurs at temperatures extending between 450 and 650°C, and thermal or physical activation using steam or CO_2 at 800 to 900°C [23].

In order to increase the capacity for adsorption by modifying the surface with sodium hydroxide (NaOH), the present work has made an effort to create highly activated hydrochar (AHC) produced from maize cobs. In contrast with potassium hydroxide (KOH), NaOH has three benefits: the least degree of corrosion, a cheaper cost, and the least

weight dose. Additionally, the byproducts of NaOH activation such as sodium carbonate (Na_2CO_3) and sodium metasilicate (Na_2SiO_3) are safe and nonhazardous. Therefore, a surface modification method including NaOH might be viewed as nontoxic to the environment [24]. Furthermore, the development of OFG on the external layer of carbon is closely related to these activation techniques. According to the literature review, chemical activation produces more OFG than physical activation. Compared to other activating agents, NaOH triggers a larger surface oxygen content to be generated during the chemical activation process [25].

The unique feature of this research is the production of AHC from maize cob leftovers using the HTC approach and the chemical modification of the HC that is currently being developed to remove anionic dyes from aqueous solutions. No one has, as of yet, reported successfully removing rose bengal dye using AHC as a sorbent.

The unique goal of this research is to develop AHC and test its efficacy in removing rose bengal dye from synthetic water systems. To evaluate the qualitative analysis of AHC, FTIR and SEM-EDAX analyses were carried out. Through batch tests, a thorough analysis of the adsorptive capability of the produced AHC was conducted. Adsorption equilibrium and kinetic research were used to estimate the sorption process of removing rose bengal dye using AHC. The nature of the sorption system has also been determined via the explanation of thermodynamic sorption investigations.

2. Protocol for Experimentation

2.1. Chemical Agents. The chemical compounds employed in this study are all of the highest quality analytical grade. Sodium hydroxide (NaOH, 97%, Thermo Fisher Scientific India Pvt Ltd), hydrochloric acid (HCl, 37%, Thermo Fisher Scientific India Pvt Ltd), rose bengal dye having the molecular formula $C_{20}H_2Na_2O_5I_4Cl_4$, and a stainless steel Teflon-lined autoclave was procured from Vijaya Scientific Company, Chennai, India.

2.2. Synthesis of Hydrochar. The biomass precursor corncob (CC) was collected locally near Madhavaram, Chennai (13.1488° N, 80.2306° E). This CC was chopped into compact chunks to bring down the size of the CC and it was further cleansed with double-distilled water to get rid of the dirt clinging into the surface of the CC. This CC sample was dried in a hot air oven at 100°C for 24 h duration to expel the moisture present in the CC sample. The moisture-free CC sample was then pulverized and sieved into a fine powder. A certain quantity (2-3 g) of this CC powder was diffused in double-distilled water (50 mL) and bolted into a 100 mL Teflon-lined autoclave which was maintained at a temperature of 180°C for 14-16 h permitting HTC reaction to occur. As a result of the HTC reaction, a brownish-black precipitate with a reddish-brown solution was obtained which was further cleansed with double-distilled water and ethanol until the solution turned colorless. The thus obtained solid products were dried at 105°C for 24 h duration [26]. The moisture-free sample was named as HC.

2.3. Synthesis of Activated Hydrochar. For the preparation of AHC, a precise quantity of HC was dispersed in 0.5 M of NaOH and was stirred at room temperature for 1 h duration. This mixture was separated using vacuum filtration, and the solid products were finally washed with double-distilled water until the pH attained a neutral value. The final product was then dried at 105°C for 24 h and was labeled as AHC which was employed for further experimental studies [27].

2.4. Characterization of HC and AHC. The as-prepared samples were characterized to affirm the emergence of HC and AHC from the CC precursor. The elemental composition and morphological structures of HC and AHC were determined by a field emission scanning electron microscope (FE-SEM) at Thermo Fisher FEI QUANTA 250 FEG. The existence of functional groups on the surface of HC and AHC was investigated using Fourier transform infrared spectroscopy (FT-IR) by making use of Spectrum Two FT-IR/Sp 10 software, Perkin Elmer, USA. The crystalline nature of HC was studied using an X-ray diffractometer (XRD), Empyrean Malvern Panalytical, the Netherlands. The Brunauer-Emmett-Teller (BET) theory was used to figure out the presence of pore size distribution and specific surface area (SSA) of the synthesized material, and the analysis was performed using Autosorb IQ, Model 6 ASiQWin version 5.00. Additionally, using the Barrett-Joyner-Halenda (BJH) approach, pore volume distribution was computed as a function of pore size.

2.5. Adsorption Studies. To examine the consistency of variables impacting the sorption procedure like time duration (2-45 min), primary solution concentration (100-500 mg/L), solution pH (2–7), and sorbent dose (0.1-0.6 g/L), a definite amount of AHC is mixed with an appropriate concentration of rose bengal dye. Then, this combination was placed inside the shaker at 100 rpm for uniform mixing. A fixed quantity of sample solution was taken out at periodic time intervals and filtered using Whatman 42 filter paper, and the sample was examined for the remaining concentration of the dye by a UV-Vis spectrophotometer (JASCO V-630) at λ_{max} = 545 nm. Rose bengal dye absorbs visible light in this region (545 nm). The following equation is used to measure the rose bengal dye uptake from aqueous solutions.

$$\text{Percentage removal of rose bengal dye} = \frac{C_o - C_e}{C_o} \times 100, \tag{1}$$

where C_o and C_e denote the initial and final concentration of rose bengal dye, respectively.

2.6. Isothermal Study for Rose Bengal Dye. Data from a batch investigation of preliminary dye concentration was used to evaluate equilibrium studies. The adsorption capability of AHC at equilibrium conditions is obtained by employing the following equation:

$$q_e = \frac{(C_o - C_e)V}{m}, \tag{2}$$

where m denotes the amount of AHC in grams (g), V represents the volume of rose bengal dye in litre (L), and C_o and C_e signify the concentration of dye at initial and equilibrium conditions in milligram per litre (mg/L).

To predict the interaction between aqueous solution and AHC adsorption, an isothermal prototype was used. Two different adsorption isotherm models have been used to evaluate adsorptive data. The MATLAB R2015a programme was used to conduct the nonlinear regression analysis and produce variables of adsorption, such as correlation coefficients and error values. The best-fitting isotherm model has been found based on the isotherm study findings.

2.6.1. Two Parameter Models. The Langmuir isothermal model is represented as shown in the following:

$$q_e = \frac{q_m K_L C_e}{1 + K_L C_e}, \tag{3}$$

where C_e represents the equilibrium concentration of rose bengal dye in mg/L, K_L denotes the Langmuir constant in L/mg, q_m denotes the maximum sorption capacity in mg/g, and q_e indicates the sorption capacity in mg/g.

The Freundlich model is represented by the equation which is shown as follows:

$$q_e = K_F C_e^{1/n}, \tag{4}$$

where K_F denotes the Freundlich constant in [(mg/g) (L/mg)$^{1/n}$] and is utilized to determine the sorption capability and the Freundlich exponent n is used to calculate the adsorption intensity. The following are the possible outcomes of n: $n < 1$, $n > 1$, and $n = 1$ denotes chemical, physical, and linear processes.

2.6.2. Three Parameter Models. The Redlich Peterson (RP) model is represented by the equation which is shown as follows:

$$q_e = \frac{K_{Rp} C_e}{1 + \alpha_{RP} C_e^{\beta_{RP}}}, \tag{5}$$

where K_{Rp} denotes the RP constant in L/g, α_{RP} represents the RP isotherm constant in (L/mg)$^{1/\beta\mathrm{RP}}$, and the exponent between 0 and 1 is called β_{RP}. The value of β is highlighted as follows:

The Freundlich adsorption isothermal model is more desirable if $\beta = 0$.

The Langmuir adsorption isothermal model is more desirable if $\beta = 1$.

The Toth model is represented by the equation which is shown in the following:

$$q_e = \frac{q_{mT} C_e}{\left(1/K_T + C_e^{mT}\right)^{1/mT}}, \tag{6}$$

where the Toth model exponent is denoted by mT, the Toth equilibrium constant is denoted by K_T, the equilibrium concentration of sorbate is denoted by C_e in mg/L, and the Toth maximum sorption capacity is denoted by q_{mT} in mg/g.

2.7. Kinetic Studies. The sorption kinetic tests were carried out in a 250 mL Erlenmeyer flask with 100 mL of the required dye solution concentration. The desired quantity of AHC was incorporated into the solution as part of this kinetic investigation, and the contact duration between the dye solution and AHC was adjusted to range from 0 to 45 minutes. The blended solution was maintained in a shaking incubator with an ideal pH and temperature controller. The experimental solutions were removed from the shaking incubator at the right time after the predetermined interval. The Whatman 42 filter paper was used to filter the leftover solutions. Finally, a UV-Vis spectrophotometer was used to calculate the concentration of leftover dye in the solution. Using the following formula, the quantity of dye adsorbed by AHC at various time intervals (q_t) (mg/g) was determined.

$$q_t = \frac{(C_o - C_t)V}{m}. \tag{7}$$

where m denotes the mass of the sorbent in grams, V denotes the volume of rose bengal dye solution in litre, C_t is the dye solution concentration expressed in mg/L at time interval t, C_o denotes the primary concentration of dye solution in mg/L, and q_t represents the quantity of dye adsorbed onto AHC at time t in mg/g.

To calculate the adsorption rate, kinetic models of pseudo-first-order, pseudo-second-order, and intraparticle diffusion (IPD) were fitted to the data obtained from the experiment.

The equation for the pseudo-first-order kinetic model is given by

$$q_t = q_e(1 - \exp(-k_1 t)), \tag{8}$$

where t represents time in min and k_1 represents pseudo-first-order kinetic rate constant in min^{-1}.

The equation for the pseudo-second-order kinetic model is given by

$$q_t = \frac{q_e^2 k_2 t}{1 + q_e k_2 t}, \tag{9}$$

where k_2 indicates the pseudo-second-order kinetic rate constant in g/mg min and t denotes time in min.

Applying the Weber-Morris IPD model, which revolves around Fick's second law of diffusion, the kinetic data was examined to define the diffusion process. The IPD model is written as

$$q_t = k_p t^{1/2} + C, \tag{10}$$

where C represents the intercept, t denotes the time in minutes, k_p indicates the IPD rate constant in mg/g/min$^{1/2}$, and q_t represents the sorption capability at time t in mg/g.

2.8. Thermodynamic Study of Rose Bengal Dye. The examination of thermodynamic variables establishes the feasibility of the sorption process, which is dependent on temperature. The characteristics of the sorption process, whether physical or chemical sorption, can only be predicted using thermodynamic analysis. Further, it aids in determining if the sorption procedure is reversible or irreversible, endothermic or exothermic, and spontaneous or nonspontaneous in nature [28].

The nature and features of the sorption procedure have been found by investigating thermodynamic parameters like enthalpy change (ΔH°, kJ/mol), Gibb's free energy (ΔG°, kJ/mol), and change in entropy (ΔS°, kJ/mol). The following formulas were used to calculate thermodynamic parameters:

$$K_c = \frac{C_{Ae}}{C_e},$$
$$\Delta G^{\circ} = -RT \ln K_c, \quad (11)$$
$$\mathrm{Log}K_c = \frac{\Delta S^{\circ}}{2.303R} - \frac{\Delta H^{\circ}}{2.303RT},$$

where C_{Ae} denotes the amount of rose bengal dye adsorbed onto corncob hydrochar per litre of solution in mg/L, C_e represents the concentration of dye solution at equilibrium condition in mg/L, T indicates the temperature in Kelvin, R denotes the universal gas constant (8.314 J/mol.K), and K_c represents the equilibrium constant. The slope and intercept of the log K_c against $1/T$ plot were used to determine the values of ΔH° and ΔS°.

3. Results and Discussions

3.1. HC and AHC Characterization

3.1.1. X-Ray Diffraction. Assessing the crystalline or amorphous nature of the prepared product requires knowledge of the XRD profile. Figure 1 displays the XRD pattern for HC. Three distinct peaks were observed at 15.3°, 22.5°, and 34.7°, respectively. As a result of the hydrolysis reaction and subsequent breakdown of cellulose at HTC temperature, peaks at 15.3° and 34.7° in the CC-HTC HC have been substituted by a wide diffraction peak at 22.5°, which is compatible with the (002) diffraction patterns of amorphous carbon. CC's XRD revealed cellulose-related diffraction peaks between 15.3° and 22.5° [29], and hemicellulose corresponds to the peak at 34.7°. The HC's 15.3° and 22° observed peaks are stronger, suggesting their aromatic nature. These increased intensities demonstrate that aromatization has grown as a result of the rise in substances like graphite. Additionally, it demonstrates that cellulose is destroyed during the HTC process [30]. Below 200°C, the HC's cellulose amount essentially remained unaltered. The cellulose content declined quickly until it vanished as the temperature rose. These findings suggest that at temperatures over 200°C, the microcrystalline structure of the CC HC started to quickly decay [31]. The microcrystalline structure was destroyed by the HTC treatment. The microcrystalline structure of the cellulose, which is consistent with the behaviour of pyrolysis, may be to blame for this [32].

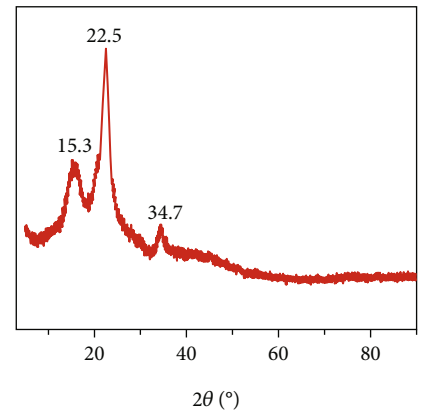

Figure 1: XRD pattern for HC.

3.1.2. Fourier Transform Infrared Spectroscopy (FTIR). The FTIR spectra of HC and AHC are depicted in Figure 2. It can be seen that the strong and broad band at 3499 cm^{-1} denotes the O-H vibration in the carboxyl and hydroxyl groups [33]. This suggested that the HTC procedure did not entirely destroy the O-H groups that were initially present in lignin, cellulose, and hemicellulose [34]. The peak at 1658 cm^{-1} is assigned to C=O stretching in the carbonyl, carboxyl groups, ester, and quinone functional groups. This implies that HTC results in the generation of functional groups featuring oxygen [35]. The peak at 1150 cm^{-1} ascribes to the C-O stretching. The reduction in these peaks affirms that dehydration has occurred during HTC [36]. The bending vibration C-H [37] occurred at 719 cm^{-1} due to the aromatization reaction [26].

Significant OFG reductions may be observed after HC has been activated with alkali in the absence of oxygen and at elevated temperatures, pointing to the possibility of a carbonization process [25]. This happened as a result of certain bonds being broken in the course of activation processes, which allowed volatile chemicals to be released and profoundly altered the surface of the material [38]. For example, the peak at 1150 cm^{-1} may have become unreadable due to the interaction of HC's carbon framework with the reducing compound NaOH, which resulted in the production of carbonates by altering the chemical framework. As a result, the peak has been moved to 1299 cm^{-1}, which is consistent with the C-O stretching of carboxylic acid [25]. The broad stretching at 2958 cm^{-1} corresponds to the C-H group [39]. The formation of the C-H groups in AHC is a result of complex chemical reactions that involve dehydration, dehydrogenation, thermal decomposition, the removal of oxygen-containing groups, the presence of aromatic structures, reductive conditions, and the depolymerization of organic polymers. The peaks emerging at 3556 and 3670 cm^{-1} indicate the O-H group in AHC [40]. This implies that the functional group featuring oxygen is present in larger amounts on the surface of AHC [20]. It is clear from the analysis that the primary functional groups on the surface that might be

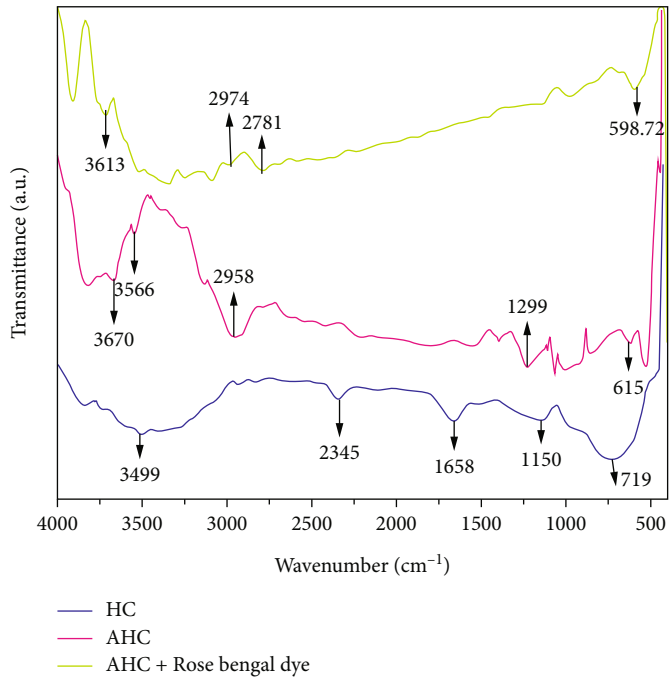

Figure 2: FTIR spectra for HC, AHC, and AHC with dye.

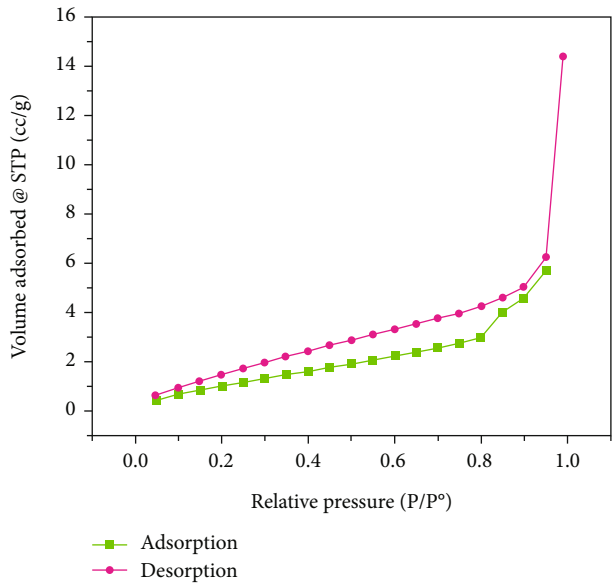

Figure 3: Adsorption-desorption isotherm for AHC.

in charge of facilitating the relationship between rose bengal dye and carbon framework following activation are the carboxylic and hydroxyl groups.

The major cause of the large absorption peak at 3613 cm^{-1} was the stretching of the O-H vibration. The C-H symmetric and asymmetric vibrations of stretch were responsible for the adsorption maxima at 2974 and 2781 cm^{-1}, respectively. Notably, a peak at 3566 cm^{-1} that appeared in AHC and strengthened in AHC along with dye (3613 cm^{-1}) may be the result of insoluble hydroxide created during the NaOH treatment procedure. Last but not least, the peak at 3670 cm^{-1} disappeared, showing that almost all of the contaminants have been cleared [41].

3.1.3. BET Analysis and Pore Size Distribution. Analysis of SSA and porosity produced following activation of HC with NaOH was done using N_2 physisorption. Figure 3 shows the N_2 adsorption and desorption isotherms for AHC at 77.35 K. The isotherm profiles reported here matched those described by Islam et al. AHC possessed a pore volume of 0.025 cc/g and SSA of 12.794 m^2/g. The pore diameter was determined to be 1.431 nm. The following is the most likely mechanism for the enhanced surface area brought on by the treatment with NaOH:

$$2C + 6NaOH \longrightarrow 2Na_2CO_3 + 2Na + 3H_2 \quad (12)$$

Sodium carbonate deteriorated into water and carbon dioxide due to additional activation at an elevated temperature in the existence of N_2 gas, which trapped them in pores and caused bigger holes [42]. The distribution of pore diameters in AHC is another crucial factor. In reality, the most crucial factor for describing the structural variability of porous materials is the pore size distribution. It serves as a prototype of a solid internal structure and is intimately connected to both the equilibrium and kinetic characteristics of these compounds [43]. The porosity of this product is totally controlled by both meso and micropores, according to the BJH method's calculation of the pores' size distribution. Figure 4 depicts the pore size distributions of AHC produced from CC at 180 degrees. As can be seen, the graph has two peaks, the largest of which has a max at 11.946 and 1.431 nm.

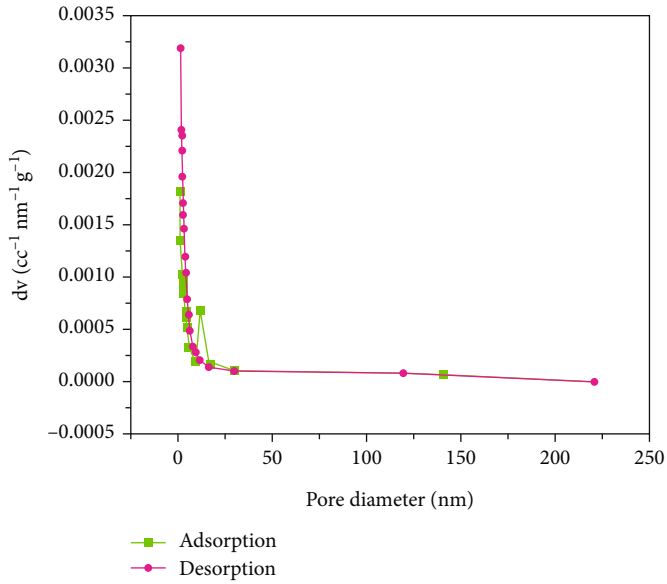

Figure 4: Pore size distribution of AHC for adsorption and desorption branch.

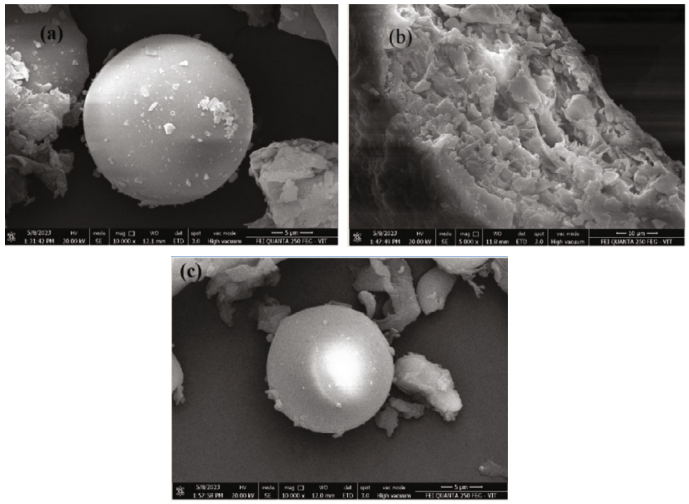

Figure 5: (a–c) Structural morphology of HC and AHC.

3.1.4. Surface Morphological Analysis. The adsorbent material's surface structure and morphology were examined using scanning electron microscopy (SEM), as seen in Figures 5(a) and 5(b). The surface of the HC was discovered to have smooth, monodisperse spheres that were created through the thermal polycondensation of cellulose, hemicellulose, and a little amount of lignin [34]. Due to the aromatization, decreolization, and dehydration processes produced by HTC treatment, the HC's surface has transformed into spherical vesicles [44].

SEM images reveal that the structural modifications of CC HC post HTC resemble those of cellulose. The size of the cellulose particles decreases as the hydrotreating temperature rises as a result of polymerization and nucleation processes, which cause various sites of the fibrous structure to break down and the production of micron-sized pieces of cellulose [45]. Due to the recondensation of volatile compounds in HTC, pore formation does not happen very much. The cell wall of the sample was primarily modified by HTC in the areas of hemicellulose, cellulose, and lignin, which changed the adsorbents' surface characteristics. These alterations in the sample's surface chemistry might facilitate the diffusion of NaOH molecules into the HC's core and increase the number of pores [42]. The nonuniformity in the average particle shape of AHC compared to HC is due to the infusion of NaOH during activation, which accelerates the breakdown of cellulose and lignin [20].

Figures 5(a) and 5(b) illustrate that HC is smooth and has few pores, while AHC is rough and has many pores. The pores in AHC make it good at adsorbing pollutants. Figure 5(c) shows that chemical treatment has very little

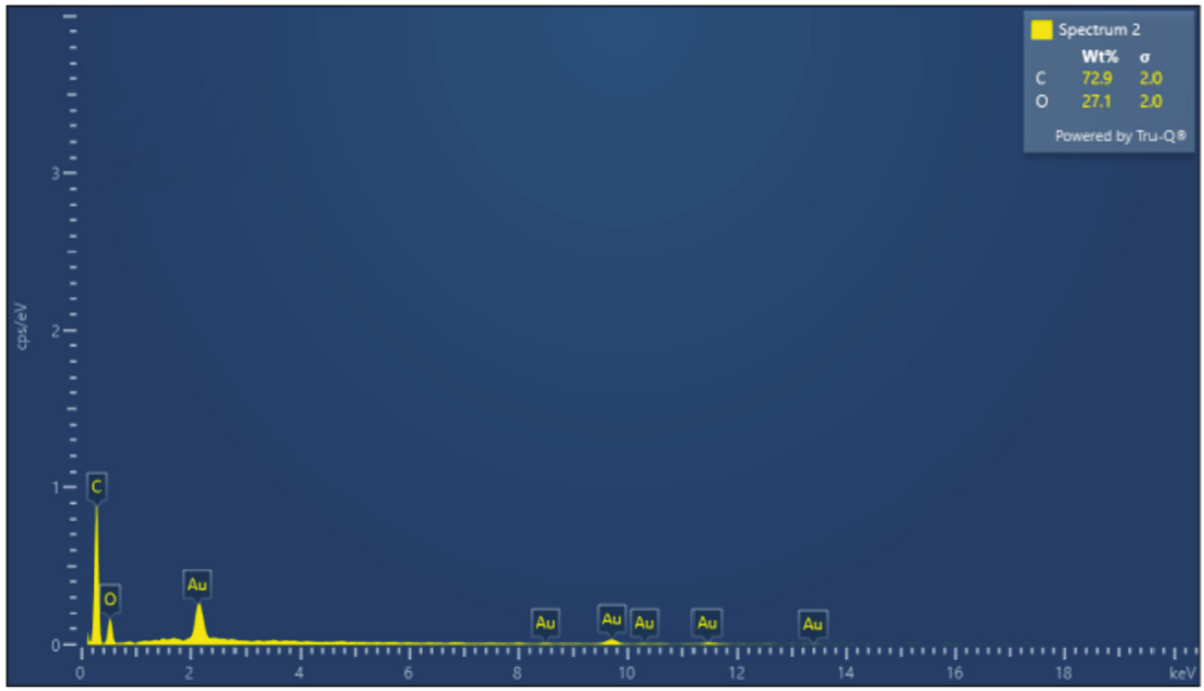

(a)

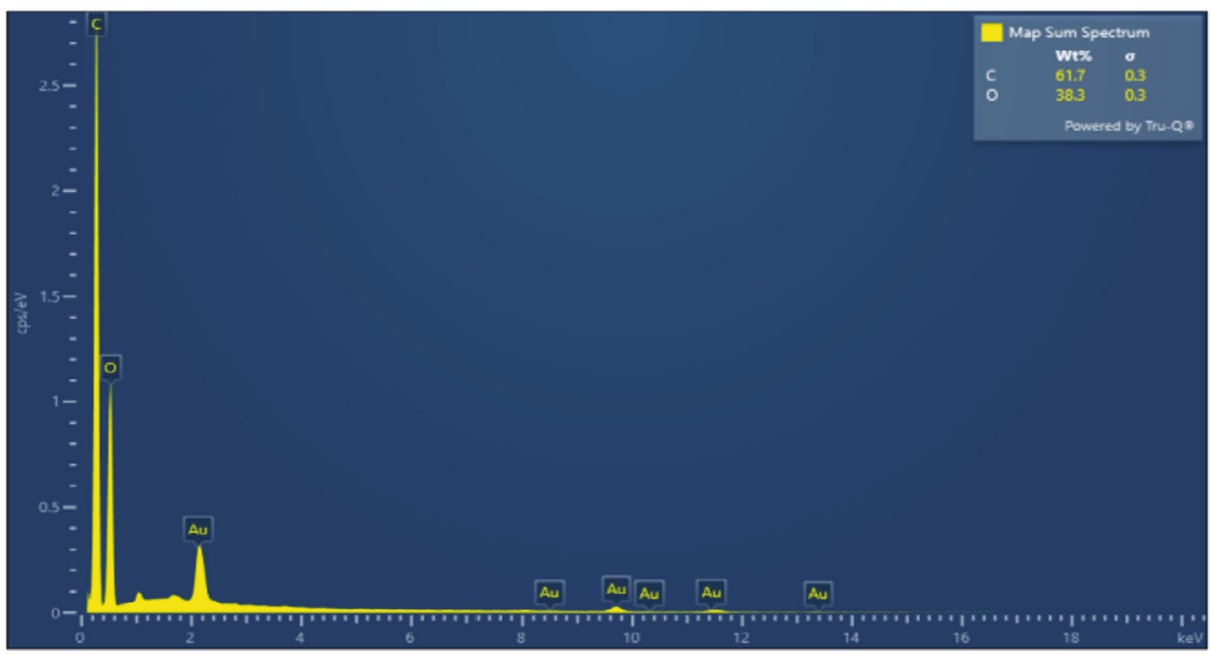

(b)

Figure 6: Continued.

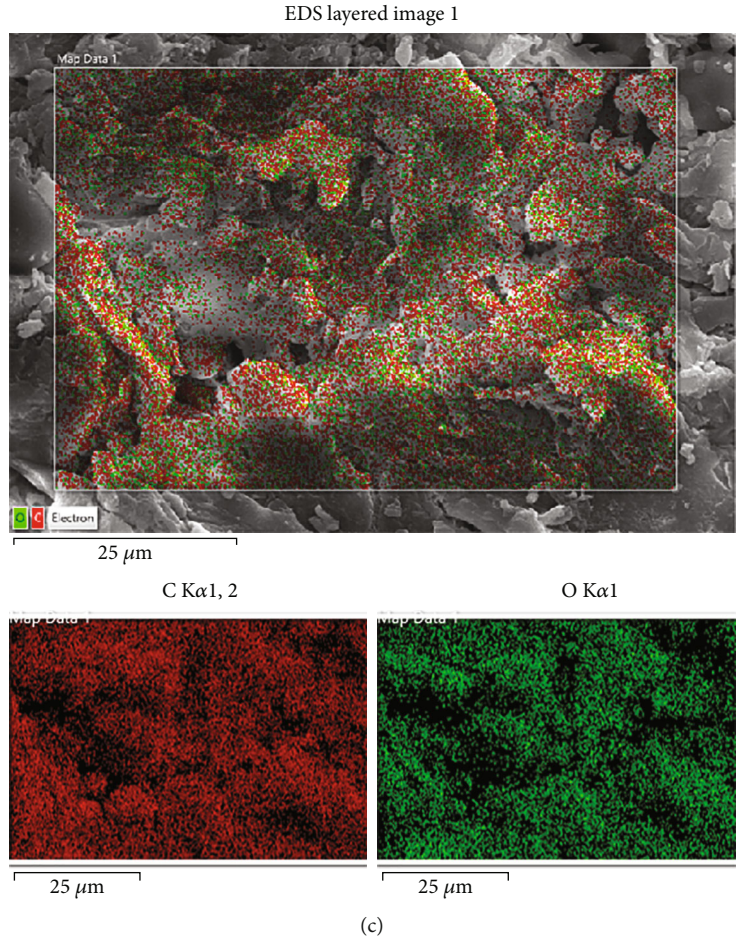

(c)

Figure 6: EDS spectra of (a) HC and (b) AHC. (c) Elemental mapping of AHC.

effect on the size of HC and AHC. The SEM picture in Figure 5(c) demonstrates that the AHC's spherical structure is similar to that of the HC. This shows that the structure of the sphere was maintained even after chemical activation [46].

3.1.5. EDS Analysis. In terms of elemental analysis, as shown in Figures 6(a) and 6(b), EDS mapping revealed that HC had a higher percentage of carbon of about 72.9 percentage and a lower percentage of oxygen of about 27.1 percentage than AHC (61.7 and 38.3, respectively). This may be explained by the fact that HTC really included the processes of decarboxylation and dehydration. Lignin, hemicellulose, and cellulose are complex polymers made of oxygen, hydrogen, and carbon, which are the three primary substances that makeup CC. For the production of HC, hemicellulose and cellulose break up into tiny units, and these are then subsequently dehydrogenated and dehydrated. Additionally, the lignin is depolymerized and transformed into HC. The oxygen atoms are eliminated, whereas the carbon and hydrogen atoms are maintained throughout this procedure. The HC is primarily composed of a carbon (C) atom framework, with hydrogen (H) atoms forming chemical bonds between C atoms, contributing to the structural stability of the HC. Oxygen atoms are removed from HC, which results in a drop in the HC's oxygen content. Furthermore, the overall makeup of HC can be impacted by specific HTC process variables, like retention time, pressure, and temperature [44]. According to the element mapping information in Figure 6(c), the C and O elements, which are highlighted in red and green, makeup AHC. Compared to the O element, the spread of the C element is greater, as can be seen from the elemental mapping.

3.2. Variables Affecting Adsorption Process

3.2.1. pH's Impact. Figure 7 illustrates the outcomes of an investigation into the impact of solution pH in the range of 2.0 to 7.0. It was discovered that when pH increased, dye elimination also increased, reaching its maximum level at pH 3.0. Because hydrogen ions and dye molecules compete for active sites on the surface at lower pH levels, dye removal was hampered. On the contrary, a higher pH resulted in a lower concentration of hydrogen ions in the solution, which made functional groups on the AHC surface deprotonated and more suited for attaching the dye molecules. A modest reduction in the adsorption of rose bengal dye was seen at a pH higher than 3.0, which is likely because the dye molecules were trying to hydrolyze and precipitate instead of being absorbed [19]. Figure 7 illustrates how pH

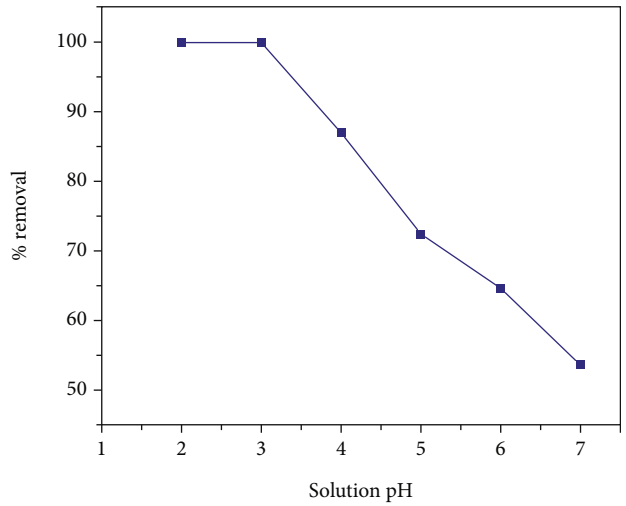

Figure 7: Rose bengal dye sorption onto AHC and the impact of pH (C_o = 100 mg/L, dosage = 0.4 g/L, contact time = 10 min, and volume = 100 mL).

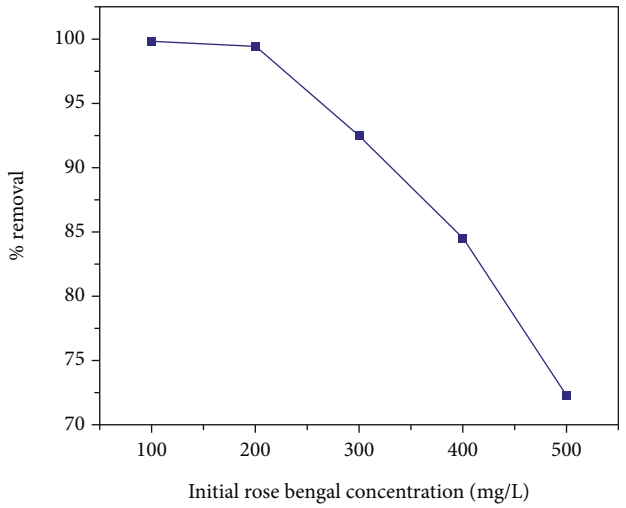

Figure 8: Effect of rose bengal dye concentration onto AHC (contact time = 10 min, dosage = 0.4 g/L, pH = 3.0, and volume = 100 mL).

affects the adsorption of rose bengal dye at primary concentrations of 100 mg/L onto AHC. Because pH affects the ionization of sorbates and the surface charge of sorbents, the solution's pH has an effect on the absorption of rose bengal dye [47]. The most crucial variable in the adsorption technique is the concentration of hydrogen ions. It regulates the adsorbent surface's protonation and deprotonation processes. At constant temperature, 100 mg/L of the rose bengal dye was combined with 0.4 g/L of the adsorbent to examine the impact of pH on the effectiveness of the dye's removal via adsorption [48]. At various pH levels between 2 and 7, AHC was tested to see how pH affected the sorption of rose bengal dye [47]. The percentage removal of the dye is higher in an acidic medium [48].

3.2.2. Primary Concentration's Impact. Adsorption ability was assessed in relation to how the preliminary dye concentration changed. When the pH was 3 and the sorbent dosage was 0.4 g/L, primary dye concentrations ranging from 100 to 500 mg/L were used to study the sorbing ability of AHC. Figure 8 shows the removal efficacy declined from 99.84% to 72.29% when the concentration of rose bengal dye spiked from 100 to 500 mg/L. The areas of sorption on the outermost layer of the adsorbent tend to get saturated when the primary dye concentration in the solution rises, which reduces the efficacy of removal. As the dye molecules that encircle the AHC grow, active sites grow as the initial concentration of dye rises, which raises the values of q_e and the mass transfer driving force [49]. In other words, a modest dye solution concentration can cover a large surface area. Additionally, the high dye solution concentration might cause adsorptive sites to overlap. As a result, at high concentrations, there are fewer dye molecules competing for binding sites on the surface of the adsorbent [50].

3.2.3. Impact of Sorbent Dose. The effects of AHC dosage on rose bengal dye elimination were investigated, and the findings are shown in Figure 9. The AHC dose ranged from 0.1 to 0.6 g at 100 mg/L dye concentration, with an interaction duration lasting 10 minutes at a pH level of 3. It was shown that the percentage of dye removal rose quickly with an increase in AHC dose up to 0.6 g, but that the addition of more AHC did not provide any noticeably different results. This is explained by the increased accessibility of the exchangeable adsorption sites. There is no apparent change in rose bengal dye removal over 0.6 g/100 mL [51]. The elimination of rose bengal dye was not enhanced anymore with a raise in adsorbent dose over 0.6 g [52].

3.2.4. Influence of Contact Time. The impact of the contact period on the expulsion of rose bengal dye was investigated for 100-500 mg/L. Figure 10 demonstrates the effect of time on dye expulsion by utilizing AHC. Raising the contact period from 0 to 45 minutes caused an upsurge in the percentage of dye removal, after which it remained constant. This illustrates how the AHC surface was saturated with active sites during the contact duration. Thus, the 10-minute equilibrium period was tested to see if it was appropriate for the existing adsorption system [53].

3.2.5. Effect of Temperature. Temperature is a crucial adsorption-influencing factor. Experiments for rose bengal dye removal were carried out at temperatures of 303, 310, 313, and 318 K, with an optimal pH of 3 and a contact period of 30 minutes. The starting metal concentration was altered from 100 to 500 mg/L. From 303 to 318 K, the temperature was enhanced, and the sorption of rose bengal dye rose from 92.36% to 99.84%. As this adsorbent is not uniform and the activation energies of sorption sites vary, it is clear from Figure 11 that adsorption is elevated with temperature. As a result, only the sorption points possessing lower activation energy were filled at low temperatures, while those with greater activation energy could only be filled at elevated temperatures [54].

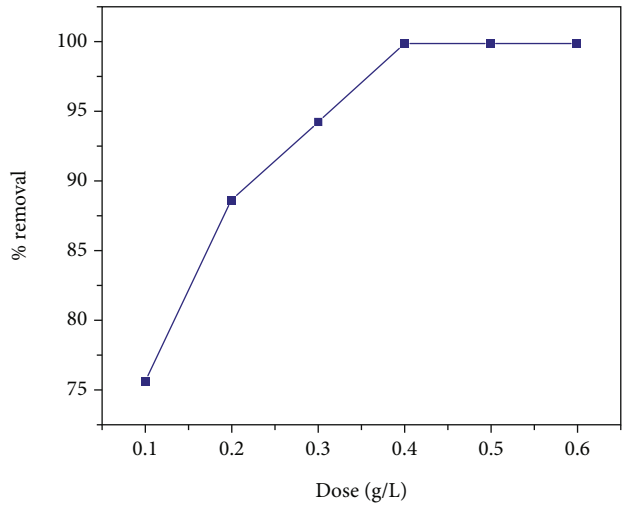

Figure 9: Impact of sorbent dosage on the sorption of rose bengal dye onto AHC (contact time = 10 min, C_o = 100 mg/L, pH = 3.0, and volume = 100 mL).

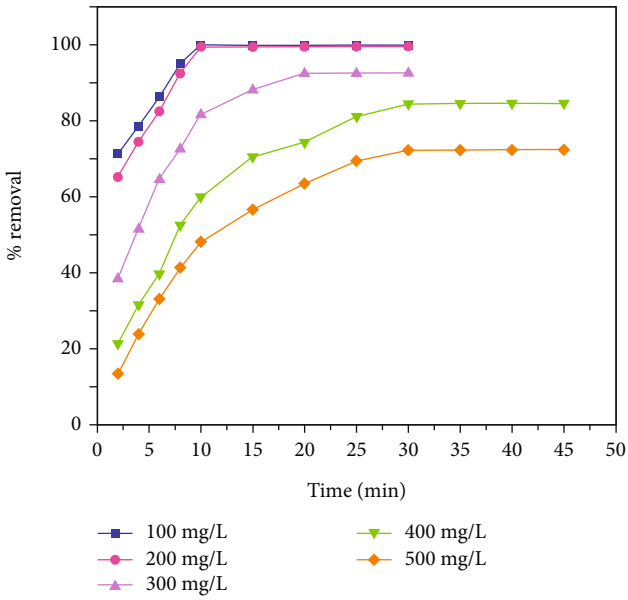

Figure 10: Influence of contact time on the sorption of rose bengal dye onto AHC (dosage = 0.4 g/L, pH = 3.0, and volume = 100 mL).

3.3. Kinetic Study. An essential tool for designing an adsorption system is adsorption kinetics. To examine the connection between adsorption rate and factors influencing the reaction, displayed in Figure 12, with various concentrations, kinetic adsorption was explored. To suit the collected empirical information, two alternative adsorption kinetic models specifically pseudo-first and second-order were applied. The graph of this data, which is a plot of q_t vs. t, is shown in Figure 12 for AHC. Table 1 is a list of the kinetic data for the rose bengal dye's sorption on AHC. Because of intense dye competition on the outermost layer of AHC, the percentage of rose bengal dye removal decreases with

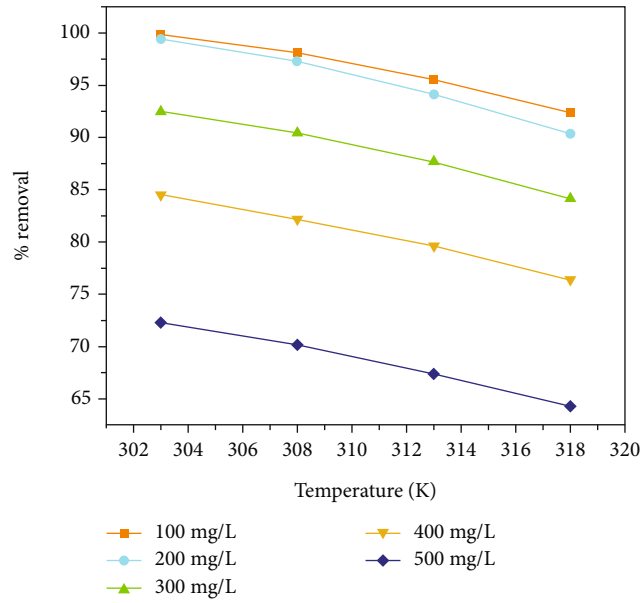

Figure 11: Effect of temperature on the sorption of rose bengal dye onto AHC (dosage = 0.4 g/L, pH = 3.0, volume = 100 mL, and time = 30 min).

increasing concentration with regard to varying contact times. According to R^2 value and the discrepancy between the estimated and observed q_e values, the best-fitting kinetic model was selected. Based on Table 1, it can be concluded that the pseudo-first-order kinetic model is the most appropriate one for the sorption of rose bengal dye because it has a higher R^2 value and because it is computed q_e value is more closely related to the observed q_e value. According to the kinetic findings, the pseudo-first-order kinetic model fits the data the best, and rose bengal dye adheres to the AHC by a physical sorption process.

The route of diffusion was identified using the IPD model and kinetic data from experiments. By employing a linear equation, the Poots, McKay, and Weber and Morris models were utilized to analyze the rate of IPD. Figure 13 indicates the formation of multiple layers. IPD and external film diffusion generally have an impact on the sorption rate. The R^2 value of the IPD model suggested that rose bengal sorption upon AHC was regulated to a certain level by IPD. q_t is mapped contrary to $t^{0.5}$ to obtain a linear line that must pass across the origin. The presence of multilinearity in the q_t vs. $t^{0.5}$ plot is taken into account. The primary stage in this process is instant sorption or external surface sorption; the subsequent step is gradual sorption, in which IPD is restrained; and the last stage denotes the final equilibrium step, in which the solute travels gradually from bigger pores to micropores, resulting in a slow sorption rate. The duration needed for the second stage is generally determined by system variables such as particle size, temperature, and concentration of the solute, and these can be difficult to forecast or manage (Feng-Chin [55]). Meanwhile, a boundary layer is obviously regulated if these lines refrain from going over the origin. When combined with

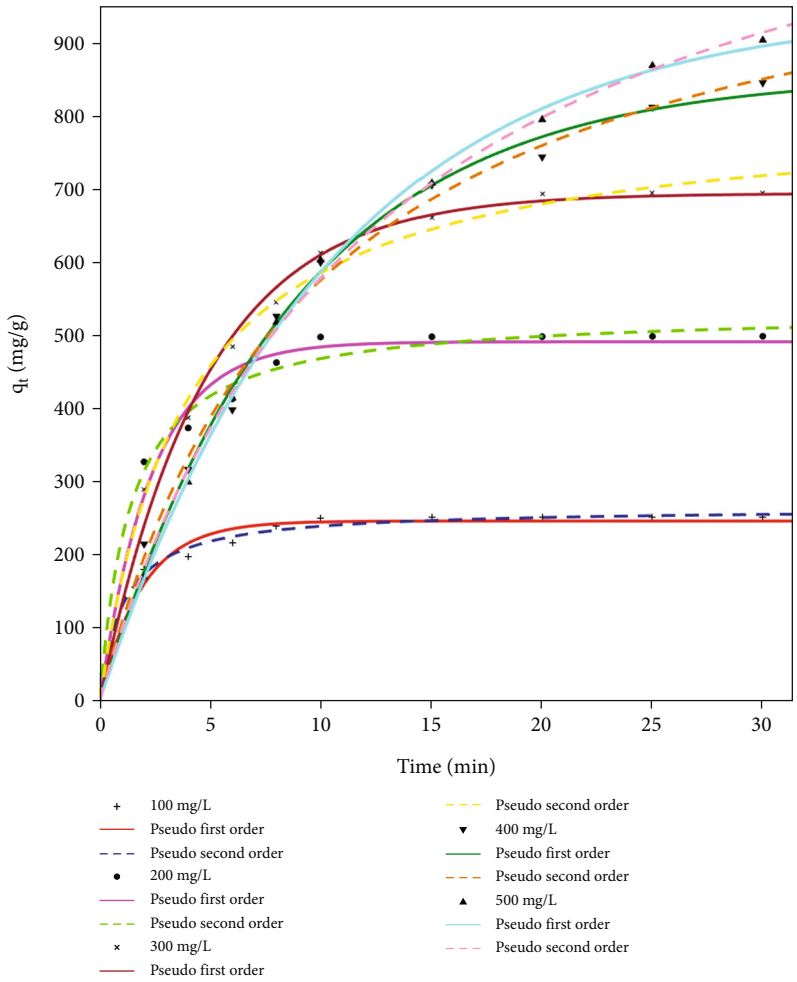

Figure 12: Kinetic models for the sorption of rose bengal dye onto AHC.

Table 1: Kinetic data for the sorption of rose bengal dye onto AHC.

C_o (mg/L)	q_e (exp) (mg/g)	Pseudo-first-order $q_t = q_e(1 - \exp(-k_1 t))$					Pseudo-second-order $q_t = q_e^2 k_2 t/1 + q_e k_2 t$				
		k_1 (min^{-1})	q_e (cal) (mg/g)	R^2	SSE	RMSE	k_2 (g/mg.min)	q_e (cal) (mg/g)	R^2	SSE	RMSE
100	250.25	0.5222	245.1	0.7954	1217	13.19	0.003618	263	0.9245	449.3	8.011
200	498.44	0.4223	490.5	0.8539	4999	26.72	0.00134	532.9	0.9338	2264	17.99
300	694.48	0.2109	693.7	0.9814	3292	21.68	0.0003202	810.2	0.9843	2776	19.91
400	846.53	0.1153	857	0.9932	3603	20.01	0.00011	1065	0.9893	5634	25.02
500	905.21	0.1012	921.8	0.9971	2021	14.99	8.343×10^{-5}	1168	0.9914	5999	25.82

other kinetic models or acting alone, it limits the sorption rate by means of IPD [50].

The Weber-Morris model, specifically IPD, was put to use to explore the rate-limiting stage in the sorption process. K and R^2 values were used to compare the pseudo-first-order model to the IPD model. The findings demonstrated that IPD was inferior to the pseudo-first-order model's R^2 value. Additionally, the fact that k_1 had a lower value than k_p suggested that the rate-limiting phase in this sorption was not diffusion. The value of k_p spiked as the primary dye concentration increased, as demonstrated in Table 2, which suggested that increasing reaction force assisted the diffusion. The variable C in the Weber-Morris equation describes the boundary layer thickness that affects the sorbent. As C increases, the boundary layer thickness also increases, highlighting the significance of the diffusion rate that cannot be disregarded. When the sorption process is governed by diffusion, the sorbate will be transported gradually across the layers and into the active sites of the sorbent [56]. Meanwhile, this study demonstrated that the sorption

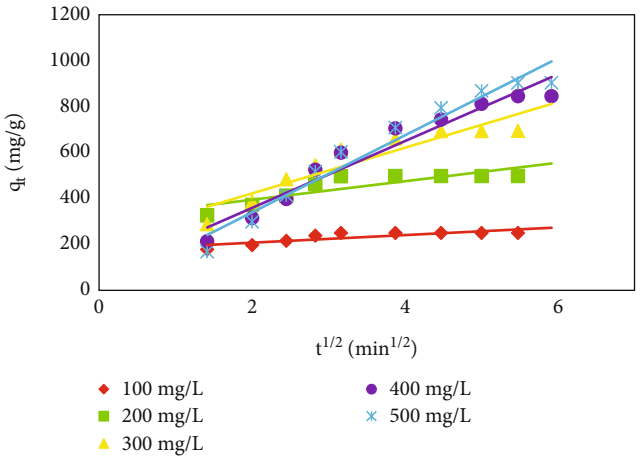

Figure 13: IPD model for sorption of rose bengal dye onto AHC.

Table 2: IPD constants for the sorption of rose bengal dye onto AHC.

C_o (mg/L)	q_e (exp) (mg/g)	IPD model $q_t = k_p t^{1/2} + C$		
		k_p (mg/(g.min)$^{(1/2)}$)	C	R^2
100	250.25	16.608	174.2	0.7155
200	498.44	40.287	313.91	0.7321
300	694.48	99.496	222.87	0.8641
400	846.53	145.49	67.895	0.9428
500	905.21	167.89	3.4818	0.9562

did not match the Weber-Morris model well, and the diffusion rate might be disregarded because of the presumption of the tiny particle size and thinner boundary layer. Intraparticle diffusion constants are listed in Table 2.

3.4. Isothermal Study. Adsorption isotherms provide insight into the relationship between sorbate and sorbent, which is important for refining the process of adsorption. As the sorption process approaches equilibrium, these equations explain the dispersion of sorbate between the solid and liquid phases. Incorporating empirical information into several isotherm models is a critical step in determining a viable model for the design of the process [57]. In this work, the equilibrium isotherm data C_e vs. q_e were evaluated using two-parameter Freundlich and Langmuir models and three-parameter RP and Toth isotherm models. The findings are displayed in Figures 14 and 15 for AHC and HC.

In order to develop some of the most popular isotherm models, such as the Freundlich isotherm and the Langmuir isotherm, it is necessary to take into account the impact of sorbate-sorbent interactions. These models rely on the presumption that the heat of sorption for every molecule in the layer declines linearly with increasing coverage of the surface. In a constant solution volume and sorbent mass, a rise in the initial dye concentration corresponds to a surge in the overall amount of dye molecules present. As a result,

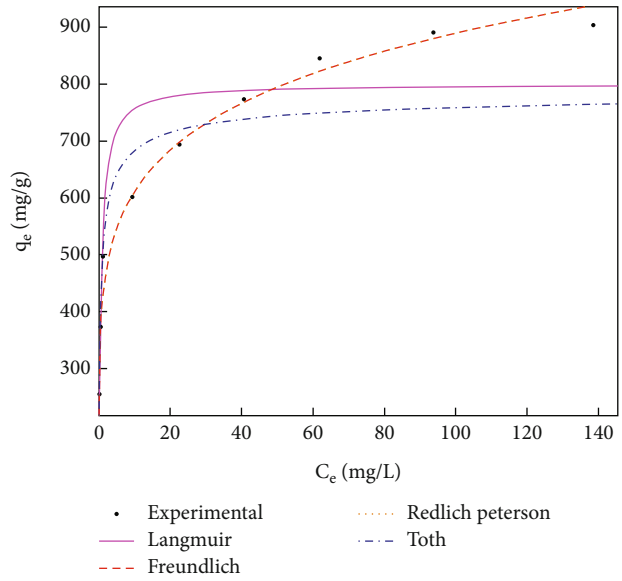

Figure 14: Isothermal models for the sorption of rose bengal dye onto AHC.

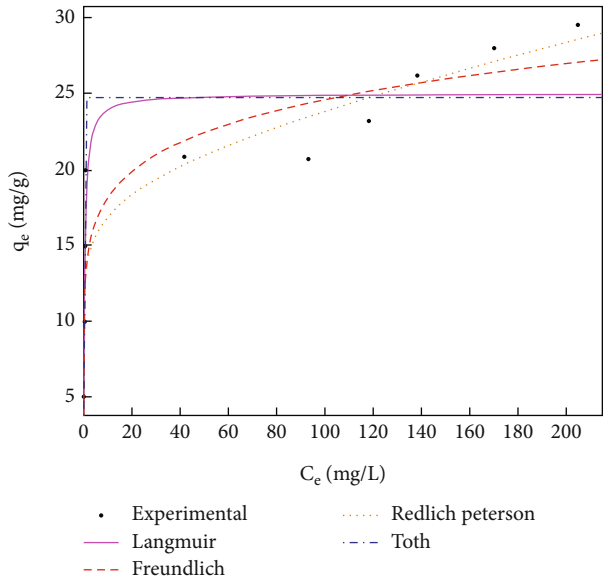

Figure 15: Isothermal models for the sorption of rose bengal dye onto HC.

at increased dye concentrations, more sorbates may adhere to the active sites on the sorbent, increasing sorption capabilities.

Generally, the Freundlich and Langmuir isotherms are all used to generally predict the results of the experimental findings for multilayer and monolayer types. To supplement the experimental investigation, the RP and Toth isothermal models were also used. The homogeneous adsorption system is described by the Langmuir isotherm, although it does not produce the most effective findings for our investigation. The Langmuir isotherm was determined to have a

Table 3: Isothermal constants for the sorption of rose bengal dye onto HC and AHC.

Isotherms	Variables	HC	AHC
Langmuir $q_e = q_m K_L C_e / 1 + K_L C_e$	K_L (L/mg)	1.739	2.199
	q_m (mg/g)	24.98	799.9
	R^2	0.8123	0.8258
	SSE	93.1	1.014×10^5
	RMSE	3.411	112.6
Freundlich $q_e = K_F C_e^{1/n}$	K_F $[(\text{mg/g})(\text{L/mg})^{1/n})]$	13.31	419.8
	n	7.508	6.133
	R^2	0.7956	0.9823
	SSE	113.4	1.029×10^4
	RMSE	3.765	35.87
Redlich Peterson $q_e = K_{Rp} C_e / 1 + \alpha_{RP} C_e^{\beta_{RP}}$	K_{Rp} (L/g)	0.03067	6.242×10^{-8}
	α_{RP} (L/mg)$(1/\beta_{\text{RP}})$	13.14	419.8
	β_{RP}	0.09919	0.1631
	R^2	0.809	0.9823
	SSE	106	1.029×10^4
	RMSE	3.892	38.35
Toth $q_e = q_{mT} C_e / \left(1/K_T + C_e^{mT}\right)^{1/mT}$	K_T	0.08412	3.404
	q_{mT} (mg/g)	24.72	793.2
	mT	42.18	0.5415
	R^2	0.8605	0.875
	SSE	77.41	7.279×10^4
	RMSE	3.326	102

Table 4: Evaluation of the AHC's maximum sorption capacity to adsorb with existing adsorbents.

S no.	Source of hydrochar	q_m (mg/g)	Reference
1.	Sugarcane bagasse	357.14	[34]
2.	Male oil palm flower	42.92	[58]
3.	Rattan furniture waste	359	[40]
4.	Corncob	183.3	[59]
5.	Corn (*Zea mays L.*)	1301.10 512.80	[60]
6.	Corncob	163.93	[61]
7.	Coffee husk	418.78	[57]
8.	Wood residues	132.1	[62]
9.	Corn starch	376.18	[63]
10.	Factory rejected tea	487.4	[64]
11.	Chili seeds	145	[65]
12.	Bamboo	655.76	[27]
13.	Palm date seed	612.1	[64]
14.	Shells of bamboo shoot	3860	[66]
15.	Corncob	799.9	This study

monolayer adsorption capacity of 799.9 mg/g for AHC and 24.98 for HC.

When applied to surfaces with heterogeneous distribution, the Freundlich isotherm model, which particularly represents the multiple-layer connection of the sorbate molecules along with the sorbent, is effective. With the Freundlich model, a comparatively high R^2 was seen for AHC. According to the relationship calculations in each model for AHC, the Freundlich equilibrium model is superior to the various selected models when it comes to applying the adsorption equilibrium of rose bengal dye. K_f values typically represent the sorbent's capability for adsorption. Greater values of K_f in this case indicate that the prepared AHC has a better capacity for multilayer adsorption. The obtained values of 7.508 (HC) and 6.133 (AHC) for the Freundlich exponent (n) indicate that AHC exhibits a higher sorption ability compared to HC.

Three variables are used by the RP isotherm to define the adsorption process. No perfect monolayer will develop, according to the RP model. Three parameters, namely, α_{RP}, β_{RP}, and K_{RP} in the RP model illustrate the equilibrium of adsorption for a wide range of sorbate concentrations. The Toth model has three more parameters that include α_{RP}, K_{RP}, and n. The Toth isotherm exponent, which was

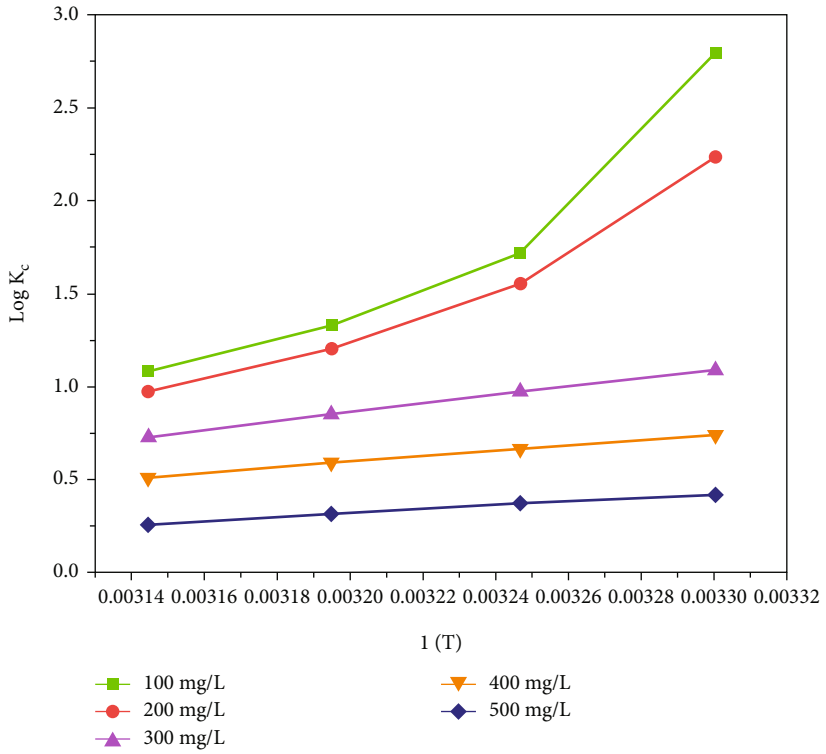

Figure 16: Thermodynamic study on the sorption of rose bengal dye on AHC.

Table 5: Parameters denoting thermodynamic values for the sorption of rose bengal dye onto AHC.

C_o (mg/L)	ΔH° (kJ/mol)	ΔS° (J/mol/K)	ΔG° (kJ/mol)			
			303 K	308 K	313 K	318 K
100	-88.95	-272.183	-16.213	-10.113	-7.956	-6.589
200	-66.493	-201.822	-12.958	-9.159	-7.211	-5.916
300	-19.444	-55.070	-6.317	-5.757	-5.109	-4.417
400	-12.056	-33.638	-4.276	-3.919	-3.547	-3.107
500	-8.641	-25.016	-2.415	-2.190	-1.886	-1.554

determined as a function of temperature, is connected to surface heterogeneity.

Table 3 illustrates the data for R^2 (correlation coefficient), SSE and RMSE (error values), and various isothermal constants for HC and AHC.

The Langmuir model analysis yielded a maximum monolayer (q_m) sorption capacity of 24.98 mg/g for HC and 799.9 mg/g for AHC. Comparing the R^2 values from Table 3, it can be inferred that the adsorption of rose bengal dye on AHC primarily involves multilayer coverage of the dye on the sorbent's surface, whereas in the case of HC, it predominantly exhibits monolayer coverage on the sorbent's surface.

Table 4 provides a comparison of AHC's sorption potential with currently accessible sorbents. The outcomes illustrated that the AHC has a strong capacity towards sorption for removing rose bengal dye from aqueous solutions.

3.5. Thermodynamic Study. The value of ΔG° was calculated as it is essential to investigate the nature of sorption and the spontaneous character of the process required for the elimination of rose bengal dye. Additionally, the physical and chemical sorption processes that are accountable for surface complexation may be distinguished using this variable. The negative value of ΔG° for the dye at all temperatures illustrates the spontaneous nature of rose bengal dye adsorption onto the exterior surface of AHC [17]. The low ΔH° value suggests an exothermic adsorption process with a poor binding capacity. This was verified by the lowering K_c values as the solution temperature increased [67]. The ΔS° value denotes the randomization of the adsorbent and rose bengal dye upon removal [68]. The thermodynamic study on the sorption of rose bengal dye on AHC is depicted in Figure 16. The value of Gibbs free energy (ΔG°), entropy (ΔS°), and enthalpy (ΔH°) is tabulated in Table 5.

3.6. Adsorption Mechanism. Rose bengal's aromatic rings can interact with the aromatic carbon structures on AHC through π-π stacking, where their π-electrons attract each other. HC's hydroxyl (-OH) groups can form hydrogen bonds with rose bengal's carbonyl (C=O) and hydroxyl (-OH) groups, strengthening the sorption through attractive forces. At certain pH levels, when AHC's carboxyl (-COOH) groups become negatively charged, they can attract and interact electrostatically with positively charged regions of rose bengal dye, aiding in its sorption onto the surface of AHC.

By considering the electrostatic attraction which exists between the sorbate and the sorbents, the sorption mechanism of rose bengal dye may be described. This can be attributed to the fact that the adsorption of the dye onto the produced sorbents is pH-dependent. Adsorbents are materials that possess a positive charge in an acidic environment when the pH drops to 2 or 3. Similar to this, rose bengal dye has a negative charge because it contains several sulfonated groups in its molecular structure. As a result, the positively charged sorbent surfaces attract the negatively charged dye molecules, enhancing the amount of dye elimination. For anionic dyes, the literature reports a similar tendency. The surface of the sorbent acquires a negative charge at elevated pH levels, which causes it to repel the dye molecule, lowering the amount of dye removal. Hence, it is evident that the electrostatic force of attraction plays a significant role in most of the absorption processes involving rose bengal dye [69].

3.7. Reusability of the AHC. Desorption tests were conducted to see if AHC could be recycled and used again as a sorbent. AHC was soaked in acidic ethanol in order to reclaim it for usage later on, and this simple solvent-washing process was used to desorb the dye. The findings of the research on the impact of 4 successive adsorption-desorption cycles is validated here. The repeated use of AHC for removing the dye was confirmed by the fact that there was only a modest decline in removal effectiveness after 4 cycles of the adsorption-desorption process. The process commenced with the initial saturation of the sorbent, where 0.1 g of AHC was stirred in a solution containing 100 mL of 100 mg/L dye for a duration of 24 h. Subsequently, the saturated AHC was subjected to agitation with an acidic ethanol solution for 3 h to facilitate desorption. Following this, the desorbed AHC was filtered, washed with deionized water, and subsequently dried in an oven at 120°C. This rejuvenated AHC was then employed once more to eliminate the dye from a solution. The regenerated AHC initially had a removal efficiency of 92.58%. Over 4 cycles of adsorption and desorption, its performance was evaluated, and the results indicated that the adsorbent remained effective for reuse up to the fourth cycle. However, during this period, the adsorption efficiency of AHC decreased from 92.58% in the first cycle to 65.17%. This decrease in efficiency could be attributed to either the blocking of active sites or a decrease in its effectiveness in removing the pollutant.

3.8. Conclusion. The research presented here shows the formed AHC produced from CC by HTC chemical activation with NaOH had good surface characteristics and worked well as a sorbent that was able to remove rose bengal dye from aqueous solutions. The carbon-rich product hydrochar was developed in the first treatment stage and had various surface functional groups because of chemical alteration with NaOH. The produced AHC was used as a highly efficient sorbent with an effective sorption capacity of 799.9 mg/g for attracting rose bengal dye. The Toth isotherm and pseudo-first-order model provided the most accurate representation of equilibrium and kinetic data. Thermodynamic analyses demonstrated the exothermic and spontaneous nature of the rose bengal dye sorption process on AHC. According to these findings, hydrochar generated by HTC and then treated with NaOH may be employed as a powerful sorbent to aid in the treatment of industrial wastewater, lowering the risk of pollutants to the environment and public health.

Data Availability

All data generated or analyzed during this study are included in this published article.

Conflicts of Interest

The authors declare that there are no conflicts of interest in this article.

Authors' Contributions

R. Sivaranjanee provided substantial contributions to the investigation, methodology, and writing—original draft. P. Senthil Kumar was responsible for the conceptualization, validation, and supervision.

References

[1] N. Mabungela, N. D. Shooto, F. Mtunzi, and E. B. Naidoo, "The adsorption of copper, lead metal ions, and methylene blue dye from aqueous solution by pure and treated fennel seeds," *Adsorption Science & Technology*, vol. 2022, Article ID 5787690, 21 pages, 2022.

[2] S. Dutta, B. Gupta, S. K. Srivastava, and A. K. Gupta, "Recent advances on the removal of dyes from wastewater using various adsorbents: a critical review," *Materials Advances*, vol. 2, no. 14, pp. 4497–4531, 2021.

[3] A. Sridhar, M. Ponnuchamy, A. Kapoor, and S. Prabhakar, "Valorization of food waste as adsorbents for toxic dye removal from contaminated waters: a review," *Journal of Hazardous Materials*, vol. 424, article 127432, Part B, 2022.

[4] M. Vinuth, H. S. Bhojya Naik, B. M. Vinoda, S. M. Pradeepa, G. Arun Kumar, and K. Chandra Sekhar, "Rapid removal of hazardous rose bengal dye using Fe(III)–montmorillonite as an effective adsorbent in aqueous solution," *Journal of Environmental & Analytical Toxicology*, vol. 6, p. 2, 2016.

[5] L. Mouni, L. Belkhiri, J.-C. Bollinger et al., "Removal of methylene blue from aqueous solutions by adsorption on kaolin: kinetic and equilibrium studies," *Applied Clay Science*, vol. 153, pp. 38–45, 2018.

[6] D. F. Romdhane, Y. Satlaoui, R. Nasraoui, A. Charef, and R. Azouzi, "Adsorption, modeling, thermodynamic, and

kinetic studies of methyl red removal from textile-polluted water using natural and purified organic matter rich clays as low-cost adsorbent," *Journal of Chemistry*, vol. 2020, Article ID 4376173, 17 pages, 2020.

[7] Y. A. B. Neolaka, Y. Lawa, J. Naat et al., "Adsorption of methyl red from aqueous solution using Bali cow bones (*Bos javanicus domesticus*) hydrochar powder," *Results in Engineering*, vol. 17, article 100824, 2023.

[8] F. Dhaouadi, L. Sellaoui, L. E. Hernández-Hernández et al., "Preparation of an avocado seed hydrochar and its application as heavy metal adsorbent: properties and advanced statistical physics modeling," *Chemical Engineering Journal*, vol. 419, article 129472, 2021.

[9] X.-N. Sun, K. Yu, J.-H. He, Y. Chen, J.-Z. Guo, and B. Li, "Multiple roles of ferric chloride in preparing efficient magnetic hydrochar for sorption of methylene blue from water solutions," *Bioresource Technology*, vol. 373, article 128715, 2023.

[10] A. Leena Pauline and K. Joseph, "Hydrothermal carbonization of organic wastes to carbonaceous solid fuel – a review of mechanisms and process parameters," *Fuel*, vol. 279, article 118472, 2020.

[11] F. N. Çatlıoğlu, S. Akay, B. Gözmen et al., "Fe-modified hydrochar from orange peel as adsorbent of food colorant brilliant black: process optimization and kinetic studies," *International journal of Environmental Science and Technology*, vol. 17, no. 4, pp. 1975–1990, 2020.

[12] S. Madduri, I. Elsayed, and E. B. Hassan, "Novel oxone treated hydrochar for the removal of Pb(II) and methylene blue (MB) dye from aqueous solutions," *Chemosphere*, vol. 260, article 127683, 2020.

[13] K. A. Phan, D. Phihusut, and N. Tuntiwiwattanapun, "Preparation of rice husk hydrochar as an atrazine adsorbent: optimization, characterization, and adsorption mechanisms," *Journal of Environmental Chemical Engineering*, vol. 10, no. 3, article 107575, 2022.

[14] M. Mäkelä, V. Benavente, and A. Fullana, "Hydrothermal carbonization of lignocellulosic biomass: effect of process conditions on hydrochar properties," *Applied Energy*, vol. 155, pp. 576–584, 2015.

[15] M. E. Malool, M. K. Moraveji, and J. Shayegan, "Optimized production, Pb(II) adsorption and characterization of alkali modified hydrochar from sugarcane bagasse," *Scientific Reports*, vol. 11, no. 1, article 22328, 2021.

[16] K. Sun, K. Ro, M. Guo, J. Novak, H. Mashayekhi, and B. Xing, "Sorption of bisphenol A, 17α-ethinyl estradiol and phenanthrene on thermally and hydrothermally produced biochars," *Bioresource Technology*, vol. 102, no. 10, pp. 5757–5763, 2011.

[17] K. Nadarajah, E. R. Bandala, Z. Zhang, S. Mundree, and A. Goonetilleke, "Removal of heavy metals from water using engineered hydrochar: kinetics and mechanistic approach," *Journal of Water Process Engineering*, vol. 40, article 101929, 2021.

[18] G. M. Khairy, A. M. Hesham, H. E. S. Jahin, S. A. El-Korashy, and Y. M. Awad, "Green synthesis of a novel eco-friendly hydrochar from pomegranate peels loaded with iron nanoparticles for the removal of copper ions and methylene blue from aqueous solutions," *Journal of Molecular Liquids*, vol. 368, article 120722, Part A, 2022.

[19] J. T. Petrović, M. D. Stojanović, J. V. Milojković et al., "Alkali modified hydrochar of grape pomace as a perspective adsorbent of Pb^{2+} from aqueous solution," *Journal of Environmental Management*, vol. 182, pp. 292–300, 2016.

[20] F. M. Jais, C. Y. Chee, Z. Ismail, and S. Ibrahim, "Experimental design via NaOH activation process and statistical analysis for activated sugarcane bagasse hydrochar for removal of dye and antibiotic," *Journal of Environmental Chemical Engineering*, vol. 9, no. 1, article 104829, 2021.

[21] X. Zhang, B. Gao, J. Fang et al., "Chemically activated hydrochar as an effective adsorbent for volatile organic compounds (VOCs)," *Chemosphere*, vol. 218, pp. 680–686, 2019.

[22] B. Chen, H. Guan, Y. Zhang et al., "Performance and mechanism of Pb2+ and Cd2+ ions' adsorption via modified antibiotic residue-based hydrochar," *Heliyon*, vol. 9, no. 4, article e14930, 2023.

[23] A. Jain, B. Rajasekhar, and M. P. Srinivasan, "Hydrothermal conversion of biomass waste to activated carbon with high porosity: a review," *Chemical Engineering Journal*, vol. 283, pp. 789–805, 2016.

[24] M. S. Hafizuddin, C. L. Lee, K. L. Chin, P. S. H'ng, P. S. Khoo, and U. Rashid, "Fabrication of highly microporous structure activated carbon via surface modification with sodium hydroxide," *Polymers*, vol. 13, no. 22, p. 3954, 2021.

[25] G. Prasannamedha, P. Senthil Kumar, R. Mehala, T. J. Sharumitha, and D. Surendhar, "Enhanced adsorptive removal of sulfamethoxazole from water using biochar derived from hydrothermal carbonization of sugarcane bagasse," *Journal of Hazardous Materials*, vol. 407, article 124825, 2021.

[26] G. Prasannamedha and P. Senthil Kumar, "Hydrothermal carbonization of waste sugarcane bagasse for the effective removal of emerging contaminants from aqueous solution," *Adsorption Science & Technology*, vol. 2022, Article ID 8684737, 13 pages, 2022.

[27] W.-C. Qian, X.-P. Luo, X. Wang, M. Guo, and B. Li, "Removal of methylene blue from aqueous solution by modified bamboo hydrochar," *Ecotoxicology and Environmental Safety*, vol. 157, pp. 300–306, 2018.

[28] T. P. Krishna Murthy, B. S. Gowrishankar, R. Hari Krishna, M. N. Chandraprabha, and B. B. Mathew, "Magnetic modification of coffee husk hydrochar for adsorptive removal of methylene blue: isotherms, kinetics and thermodynamic studies," *Environmental Chemistry and Ecotoxicology*, vol. 2, pp. 205–212, 2020.

[29] L. Zhang, J. Tan, G. Xing, X. Dou, and X. Guo, "Cotton stalk-derived hydrothermal carbon for methylene blue dye removal: investigation of the raw material plant tissues," *Bioresources and Bioprocessing*, vol. 8, no. 1, p. 10, 2021.

[30] A. Shakiba, A. Aliasghar, K. Moazeni, and M. Pazoki, "Hydrothermal carbonization of sewage sludge with sawdust and corn stalk: optimization of process parameters and characterization of hydrochar," *BioEnergy Research*, 2023.

[31] L. Yang, H. Wang, J. Sun et al., "Effects of process parameters on the physicochemical properties of corn stalk hydrochar and the removal of alkali and alkaline earth metals," *IET Renewable Power Generation*, vol. 15, no. 7, pp. 1397–1407, 2021.

[32] L. Zhang, S. Liu, B. Wang, Q. Wang, G. Yang, and J. Chen, "Effect of residence time on hydrothermal carbonization of corn cob residual," *BioResources*, vol. 10, no. 3, pp. 3979–3986, 2015.

[33] L. Xie, K. Ding, Y. Liu, M. Zou, and C. Han, "Experimental, thermodynamic and kinetic studies for the adsorption of phenolic compounds derived from oilfield wastewater by the corncob hydrochar," *Open Journal of Yangtze Oil and Gas*, vol. 4, no. 4, pp. 285–300, 2019.

[34] F. Zhou, K. Li, F. Hang et al., "Efficient removal of methylene blue by activated hydrochar prepared by hydrothermal carbonization and NaOH activation of sugarcane bagasse and phosphoric acid," *RSC Advances*, vol. 12, no. 3, pp. 1885–1896, 2022.

[35] C. Kang, L. Zhu, Y. Wang, Y. Wang, K. Xiao, and T. Tian, "Adsorption of basic dyes using walnut Shell-based biochar produced by hydrothermal carbonization," *Chemical Research in Chinese Universities*, vol. 34, no. 4, pp. 622–627, 2018.

[36] L. Zhang, Q. Wang, B. Wang, G. Yang, L. A. Lucia, and J. Chen, "Hydrothermal carbonization of corncob residues for hydrochar production," *Energy & Fuels*, vol. 29, no. 2, pp. 872–876, 2015.

[37] T. Zhang, X. Wu, X. Fan, D. C. W. Tsang, G. Li, and Y. Shen, "Corn waste valorization to generate activated hydrochar to recover ammonium nitrogen from compost leachate by hydrothermal assisted pretreatment," *Journal of Environmental Management*, vol. 236, pp. 108–117, 2019.

[38] K. C. Bedin, A. C. Martins, A. L. Cazetta, O. Pezoti, and V. C. Almeida, "KOH-activated carbon prepared from sucrose spherical carbon: adsorption equilibrium, kinetic and thermodynamic studies for methylene blue removal," *Chemical Engineering Journal*, vol. 286, pp. 476–484, 2016.

[39] M. Tabassum, M. Bardhan, T. M. Novera, M. A. Islam, A. Hadi Jawad, and M. A. Islam, "NaOH-activated betel nut husk hydrochar for efficient adsorption of methylene blue dye," *Water, Air, & Soil Pollution*, vol. 231, no. 8, p. 398, 2020.

[40] M. A. Islam, M. J. Ahmed, W. A. Khanday, M. Asif, and B. H. Hameed, "Mesoporous activated carbon prepared from NaOH activation of rattan (*Lacosperma secundiflorum*) hydrochar for methylene blue removal," *Ecotoxicology and Environmental Safety*, vol. 138, pp. 279–285, 2017.

[41] C. He, H. Lin, L. Dai et al., "Waste shrimp shell-derived hydrochar as an emergent material for methyl orange removal in aqueous solutions," *Environment International*, vol. 134, article 105340, 2020.

[42] M. Azharul Islam, A. Benhouria, M. Asif, and B. H. Hameed, "Methylene blue adsorption on factory-rejected tea activated carbon prepared by conjunction of hydrothermal carbonization and sodium hydroxide activation processes," *Journal of the Taiwan Institute of Chemical Engineers*, vol. 52, pp. 57–64, 2015.

[43] H. Hadoun, Z. Sadaoui, N. Souami, D. Sahel, and I. Toumert, "Characterization of mesoporous carbon prepared from date stems by H_3PO_4 chemical activation," *Applied Surface Science*, vol. 280, pp. 1–7, 2013.

[44] A. A. Goyi, N. M. Sher Mohammad, and K. M. Omer, "Preparation and characterization of potato peel derived hydrochar and its application for removal of Congo red: a comparative study with potato peel powder," *International Journal of Environmental Science and Technology*, 2023.

[45] O. Arellano, M. Flores, J. Guerra, A. Hidalgo, D. Rojas, and A. Strubinger, "Hydrothermal carbonization (HTC) of corncob and characterization of the obtained hydrochar," *Chemical Engineering Transactions*, vol. 50, p. 2283, 2016.

[46] H. N. Tran, F.-C. Huang, C.-K. Lee, and H.-P. Chao, "Activated carbon derived from spherical hydrochar functionalized with triethylenetetramine: synthesis, characterizations, and adsorption application," *Green Processing and Synthesis*, vol. 6, no. 6, p. 6, 2017.

[47] P. L. Homagai, R. Poudel, S. Poudel, and A. Bhattarai, "Adsorption and removal of crystal violet dye from aqueous solution by modified rice husk," *Heliyon*, vol. 8, no. 4, article e09261, 2022.

[48] M. Saleh, Z. Bilici, Y. Ozay, E. Yabalak, M. Yalvac, and N. Dizge, "Green synthesis of *Quercus coccifera* hydrochar in subcritical water medium and evaluation of its adsorption performance for BR18 dye," *Water Science & Technology*, vol. 83, no. 3, pp. 701–714, 2021.

[49] N. S. Ali, N. M. Jabbar, S. M. Alardhi, H. S. Majdi, and T. M. Albayati, "Adsorption of methyl violet dye onto a prepared bio-adsorbent from date seeds: isotherm, kinetics, and thermodynamic studies," *Heliyon*, vol. 8, no. 8, article e10276, 2022.

[50] S. Suganya and P. Senthil Kumar, "Kinetic and thermodynamic analysis for the redemption of effluents containing solochrome black T onto powdered activated carbon: a validation of new solid- liquid phase equilibrium model," *Journal of Molecular Liquids*, vol. 259, pp. 88–101, 2018.

[51] A. H. Jawad, R. Razuan, J. N. Appaturi, and L. D. Wilson, "Adsorption and mechanism study for methylene blue dye removal with carbonized watermelon (*Citrullus lanatus*) rind prepared *via* one-step liquid phase H_2SO_4 activation," *Surfaces and Interfaces*, vol. 16, pp. 76–84, 2019.

[52] A. H. Jawad, A. S. Abdulhameed, and M. S. Mastuli, "Acid-factionalized biomass material for methylene blue dye removal: a comprehensive adsorption and mechanism study," *Journal of Taibah University for Science*, vol. 14, no. 1, pp. 305–313, 2020.

[53] A. Saravanan, P. Senthil Kumar, D.-V. N. Vo et al., "Ultrasonic assisted agro waste biomass for rapid removal of cd(II) ions from aquatic environment: mechanism and modelling analysis," *Chemosphere*, vol. 271, article 129484, 2021.

[54] L. K. Asadullah and K. Tohdee, "Adsorption of hexavalent chromium onto alkali-modified biochar derived from *Lepironia articulata*: a kinetic, equilibrium, and thermodynamic study," *Water Environment Research*, vol. 91, no. 11, pp. 1433–1446, 2019.

[55] F.-C. Wu, R.-L. Tseng, and R.-S. Juang, "Initial behavior of intraparticle diffusion model used in the description of adsorption kinetics," *Chemical Engineering Journal*, vol. 153, no. 1-3, pp. 1–8, 2009.

[56] D. I. Lestari, A. T. Yuliansyah, and A. Budiman, "Adsorption studies of KOH-modified hydrochar derived from sugarcane bagasse for dye removal: kinetic, isotherm, and thermodynamic study," *Communications in Science and Technology*, vol. 7, no. 1, pp. 15–22, 2022.

[57] T. H. Tran, A. H. Le, T. H. Pham et al., "Adsorption isotherms and kinetic modeling of methylene blue dye onto a carbonaceous hydrochar adsorbent derived from coffee husk waste138325," *Science of the Total Environment*, vol. 725, 2020.

[58] A. Said, S. Tekasakul, and K. Phoungthong, "Investigation of hydrochar derived from male oil palm flower: characteristics and application for dye removal," *Polish Journal of Environmental Studies*, vol. 29, no. 1, pp. 807–815, 2020.

[59] A. H. Jawad, M. Bardhan, M. A. Islam et al., "Insights into the modeling, characterization and adsorption performance of mesoporous activated carbon from corn cob residue *via* microwave-assisted H_3PO_4 activation," *Surfaces and Interfaces*, vol. 21, article 100688, 2020.

[60] M. J. Ahmed, M. Danish, I. Anastopoulos, and K. O. Iwuozor, "Recent progress on corn (*Zea mays* L.)-based materials as raw, chemically modified, carbonaceous, and composite

adsorbents for aquatic pollutants: A review," *Journal of Analytical and Applied Pyrolysis*, vol. 172, article 106004, 2023.

[61] H. Ma, J.-B. Li, W.-W. Liu, M. Miao, B.-J. Cheng, and S.-W. Zhu, "Novel synthesis of a versatile magnetic adsorbent derived from corncob for dye removal," *Bioresource Technology*, vol. 190, pp. 13–20, 2015.

[62] J. G. da Silva Andrade, C. E. Porto, W. M. Moreira, V. R. Batistela, and M. H. N. Olsen, "Production of hydrochars from *Pinus caribaea* for biosorption of methylene blue and tartrazine yellow dyes," *Cleaner Chemical Engineering*, vol. 5, article 100092, 2023.

[63] H. Mittal, S. M. Alhassan, and S. S. Ray, "Efficient organic dye removal from wastewater by magnetic carbonaceous adsorbent prepared from corn starch," *Journal of Environmental Chemical Engineering*, vol. 6, no. 6, pp. 7119–7131, 2018.

[64] M. A. Islam, I. A. W. Tan, A. Benhouria, M. Asif, and B. H. Hameed, "Mesoporous and adsorptive properties of palm date seed activated carbon prepared via sequential hydrothermal carbonization and sodium hydroxide activation," *Chemical Engineering Journal*, vol. 270, pp. 187–195, 2015.

[65] A. Parra-Marfíl, R. Ocampo-Pérez, V. H. Collins-Martínez et al., "Synthesis and characterization of hydrochar from industrial *Capsicum annuum* seeds and its application for the adsorptive removal of methylene blue from water," *Environmental Research*, vol. 184, article 109334, 2020.

[66] Y. Liang, G. Huang, Q. Zhang, Y. Yang, J. Zhou, and J. Cai, "Hierarchical porous carbons from biowaste: hydrothermal carbonization and high-performance for rhodamine B adsorptive removal," *Journal of Molecular Liquids*, vol. 330, article 115580, 2021.

[67] B. Ghanim, T. F. O'Dwyer, J. J. Leahy et al., "Application of KOH modified seaweed hydrochar as a biosorbent of vanadium from aqueous solution: characterisations, mechanisms and regeneration capacity," *Journal of Environmental Chemical Engineering*, vol. 8, no. 5, article 104176, 2020.

[68] R. V. Hemavathy, A. Saravanan, P. Senthil Kumar, D.-V. N. Vo, S. Karishma, and S. Jeevanantham, "Adsorptive removal of Pb(II) ions onto surface modified adsorbents derived from *Cassia fistula* seeds: optimization and modelling study," *Chemosphere*, vol. 283, article 131276, 2021.

[69] S. Nirmaladevi and P. N. Palanisamy, "Adsorptive behavior of biochar and zinc chloride activated hydrochar prepared from Acacia leucophloea wood sawdust: kinetic equilibrium and thermodynamic studies," *Desalination and Water Treatment*, vol. 209, pp. 170–181, 2021.